Journal of Sound and Vibration 329 (2010) 21–42

Contents lists available at ScienceDirect

Journal of Sound and Vibration

journal homepage: www.elsevier.com/locate/jsvi

Bayesian estimation of a dynamic structure's response

Giorgio Calanni Fraccone *, Vitali Volovoi, Massimo Ruzzene

School of Aerospace Engineering, Georgia Institute of Technology, Atlanta, GA 30332, United States

ARTICLE INFO

Article history:
Received 16 December 2008
Received in revised form
21 August 2009
Accepted 26 August 2009
Handling Editor: C.L. Morfey
Available online 7 October 2009

ABSTRACT

This study focuses on the estimation of uncertainty associated with the stress/strain prediction procedures from dynamic test data of structural systems. An accurate prediction of the maximum response levels for physical components during in-field operating conditions is essential for evaluating their performance and life characteristics, as well as for investigating their behavior in light of system design and reliability assessment. Stress/strain inference for a dynamic system is based on the combination of experimental data and results from the analytical/numerical model of the component under consideration. Both modeling challenges and testing limitations contribute to the introduction of various sources of uncertainty within the given estimation procedure with consequent reduced confidence in the predicted response.

The objective of this work is to quantify the uncertainties present in the current response estimation process by means of a Bayesian-network representation of the modeling process which allows for a rigorous synthesis of modeling assumptions and information from experimental data, as it takes into account the multi-directional nature of uncertainty propagation. More specifically, the focus is on the residual uncertainty associated with the system's inferred response, and its dependence upon the amount of test data being included in the estimation analysis.

Both discrete and linear Gaussian networks were investigated with a focus on their training accuracy and performance in the presence of nonlinear relationships among the physical quantities, weak cause–effect nodal links, as well as different sensitivity levels with respect to infused evidence.

1. Introduction

The predictive accuracy of a system model is affected by uncertainty introduced by simplifying assumptions, lack of complete knowledge about the physical unit, varying accuracy associated with experimental setups and instrumentation, or other closely related causes. To improve model prediction fidelity, test data are usually correlated with model results for calibration purposes even as the former are affected by uncertainties and errors. As a result, it becomes essential to assess a system's predictive accuracy when several sources of uncertainty, both from modeling and test analysis, are combined together. This research is focused on the probabilistic description of uncertainty present in dynamic structural response predictions.

* Corresponding author.
E-mail address: gcalanni.ae04@gtalumni.org (G. Calanni Fraccone).

0022-460X/$ - see front matter © 2008 Elsevier Ltd. All rights reserved.
doi:10.1016/j.jsv.2009.08.032

A generic parametric form of a model describing the interdependencies among the various physical quantities is given by

$$\mathbf{g}(\mathbf{z}, \boldsymbol{\theta}) = \mathbf{0} \tag{1}$$

where $\mathbf{g}$ represents a $\boldsymbol{\theta}$-parameterized system of equations, of possibly various natures (e.g., algebraic, differential, or integral), describing the relationships between the physical quantities in the vector $\mathbf{z}$, while $\boldsymbol{\theta}$ is a set of parameters whose values are usually unknown *a priori*.

In order to describe complex systems and their dynamics one needs to find the proper representation in terms of the physical quantities to be included within $\mathbf{z}$, the relationships $\mathbf{g}$ linking them, and the parameter vector $\boldsymbol{\theta}$ itself. In the literature, system identification refers to the methods and approaches developed to perform the task of describing an observed system via analytical/numerical models. As suggested by [1], these methods can be grouped in three categories: white-box, black-box and gray-box models. For the white-box models, there exists a good understanding of the system or process being investigated through which an appropriate physics-based model $\mathbf{g}$ can be rigorously formulated or selected. In this case, system identification translates into the subproblem of parameter estimation for the values of $\boldsymbol{\theta}$ that best correlate the mathematical model to reality. To this end, the classical methods of least squares and statistically equivalent maximum likelihood have been long used [2,3]. Black-box approaches are data-driven and come into play when the cause–effect relationships describing a system or a process cannot be readily identified. These techniques consist of mapping a system's inputs to its outputs based exclusively on the observed/measured data. Data fitting is at the core of this type of system identification, and approaches based on response surfaces [4] or neural networks [5,6] have been proposed. Finally, gray-box models represent a combination of the previous two types. Extensive surveys on system identification techniques applied to structural dynamics are given in [1,3,7–10], where time-domain, frequency-domain, modal-based, parameter-estimation and data-fitting approaches are discussed and compared.

As part of system identification, model updating techniques rely on the information regarding observable quantities for identification of a suitable model within a class of plausible system representations, and for fine-tuning the parameters of that specific representation to better match its response predictions with the measurement data. In the past decades, various approaches have been developed for updating finite-element structural models, a survey of which can be found in [11]. Some of these techniques consist in the optimization of an objective metric, a function of certain model parameters, through standard optimization schemes, like genetic algorithms or simulated annealing [12,13]. According to [14], however, a distinction between model parameters and model structure, both of which contribute to modeling uncertainty, is deemed necessary in the problem of model updating. In fact, the concern raised is that an update performed only on model parameters may cause the adjusted quantities to no longer carry a physical meaning when their correction is in response to errors and discrepancies with test data for which they are not ultimately responsible.

Uncertain model accuracy, quality of the measurements, and limited quantity of the observed information with respect to a model's level of detail in system identification and model updating often lead to ill-conditioning and solution nonuniqueness. To address these challenges, statistical inference has been proposed since the 1970s with the idea of superimposing a probabilistic model upon a deterministic structural model [15]. More recently, the use of Bayesian statistics has been suggested to construct a framework for model updating where the aforementioned issues are addressed by considering a class of structural models together with probability models, for parameter and prediction uncertainties, which are then updated using the available test data via Bayes' theorem [16,17]. In this context, the plausibility of each structural model, within the chosen class, becomes a function of the available data, according to which either a single most probable and optimal model can be determined (in the case of global identifiability [18]), or several optimal sets of parameters' values and corresponding optimal models exist (in the case of local identifiability [18]), whose contributions are weight-averaged to produce a system's mean prediction of the response. Hence, rather than adopting a single model in the presence of multiple choices, this approach addresses the problems of solution non-uniqueness and ill-conditioning by weighing the relative importance of each model according to their plausibility with respect to the observed data, and by assigning a variance to the mean response which accounts for the lack of global identifiability and solution uniqueness. This technique has been employed, for instance, in the field of health monitoring and damage detection where a time-dependent probabilistic damage measure is constantly updated via newly collected measurements [17,19–23]. It has also been tailored to address various scenarios of measured-data incompleteness, such as unmeasured input conditions and limited number of measured degrees of freedom [22,24].

For the purpose of model updating and model prediction assessment, direct uncertainty propagation is well established. In this context, the probability distributions of certain input parameters of a system are assumed to be known and are employed to compute a corresponding probability distribution for its response. Knowledge of parameter uncertainty, however, may not always be readily available from inspection and/or measurements (e.g., a particular parameter might not be directly measured), therefore any assumption on its statistical nature could be misleading. In [25,26], an inverse method is suggested to extract the missing information on parameter uncertainty from the measurement data themselves. The technique consists of assigning a parametric family of probability distribution functions to the system inputs of interest, and of constructing an output-measurement-based likelihood function to be maximized with respect to the parameters characterizing that family. The process identifies a single probability function that best agrees with the given test data, and provides a statistical representation for the system input parameters' uncertainty.

While providing insight on parameter uncertainty, the method in [25,26] does not take into consideration the issues of modeling and measurement variability, which impact the quality of the gathered knowledge. These aspects have been addressed in [27,28] where a stochastic model-updating approach was developed to account explicitly for such uncertainty sources. Given a set of system outputs, multiple data sets of their experimental observations, obtained from seemingly identical yet distinct structures due to manufacturing variability, are statistically compared against multiple sets of their simulated predictions, generated through *a priori* uncertainties in a chosen set of model parameters. Their reconciliation provides the system input parameters' *a posteriori* statistical information quantifying the modeling uncertainty as well as taking into consideration the experimental variabilities. Finally, in dealing with the assessment of model uncertainty in model updating, an important issue is the independence of the observations. In particular, when model prediction errors are accounted for in the updating process, it was shown that the correlation existing among their different realizations reduces, *de facto*, the amount of information contained in them [29]. When ignored, this loss of information is deemed to potentially lead to misleading predictions by the system model identified as the most likely.

Model validation, closely related to model updating, also makes use of experimental data, although for a different purpose, which is the evaluation of model prediction capabilities instead of model tuning. Validation and consequent response predictability of a system are evaluated by means of a correlation assessment of test data versus simulated results for the same scenario, where a model is arguably assumed to be validated as long as it is capable of replicating the measurement data themselves [30,31]. This approach offers no guarantee that the validated model at hand can indeed predict accurately outside of the tested region [31]. Furthermore, the experimental data used for validation are affected by uncertainty, thus requiring results to be characterized, once more, in a statistical fashion. In some cases, this uncertainty is simply included within the already preexisting modeling uncertainty [30], where experimental results are, instead, treated as the reference condition. In other circumstances, selection from competing models is performed by means of statistical hypothesis testing on a given metric, according to which a proposed analytical model is either accepted or rejected based on observed data affected by errors.

In [32–35] the Bayes factor has been used in the context of system model verification and validation, while examples are offered in [36,37] on how it can also be utilized to address the lack of knowledge, referred to as statistical uncertainty [37], about the uncertainty models themselves (e.g., unknown type of probability distribution and unknown values of its parameters). In fact, given a set of observed data, a host of probability-distribution models may be considered for fitting those data. In the presence of competing models, the Bayes factor has been shown to facilitate the selection process when other goodness-of-fit metrics prove to be inconclusive in determining which probability distribution is best suited with respect to the observations [37]. Inasmuch as the Bayes factor is constructed upon some prior knowledge about the problem at hand and constitutes a metric to perform comparisons, various alternative definitions of it have been put forth in the literature to address both the issue of incomplete/missing priors and the problem of having to compare "apples" to "oranges" (i.e., comparison and selection between disjoint sets of models) [36]. Finally, when performing a comparison among competing models, attention must be given not only to the quality of data fitting, but also to the parameter complexity of the chosen model class; more complex models can better fit a data set, but may lead to poor prediction results [38,39]. The Ockham's Razor and its quantitative formulations provide a means to favor the selection of simple parameter models over complicated ones [38–41], where such a behavior has been observed to be already embedded within Bayes' rule [39].

The scope of this work is to investigate a statistical scheme for the reconciliation of experimental data and analytical results aimed at integrating heterogeneous types of uncertainties with the primary goal of quantifying and reducing the variability affecting a dynamic system's output/response estimates. The proposed methodology, applied to a specific structural inference technique, is presented next, while findings are provided for two types of Bayesian networks and a three-dimensional plate. Finally, the procedure is evaluated against the set of experimental results analyzed in [42] for the same plate structure.

2. Technical approach: inference via Bayesian networks

The proposed methodology provides a structured and coherent way to correlate and merge different sources of information to help enhance the quality of the estimation and the assessment of uncertainty. To this end, the following steps can be identified:

1. isolation, whenever possible, of the sources of uncertainty associated with different contributors (in this context, analytical model and experiments);
2. parameterization of the system's model with respect to the given sources of uncertainty;
3. identification of the main contributors to uncertainty by means of a sensitivity analysis conducted on the system's model and aimed at filtering out those factors that weakly influence the observed uncertainty;
4. assessment of the level of uncertainty present in experimental data sets via model/test correlation analysis;
5. probabilistic representation of uncertain quantities within a Bayesian-network-based response inference scheme;
6. assessment of the impact of the considered uncertainty sources upon system's accuracy; and
7. uncertainty reduction based on the information obtained from (additional) experiments.

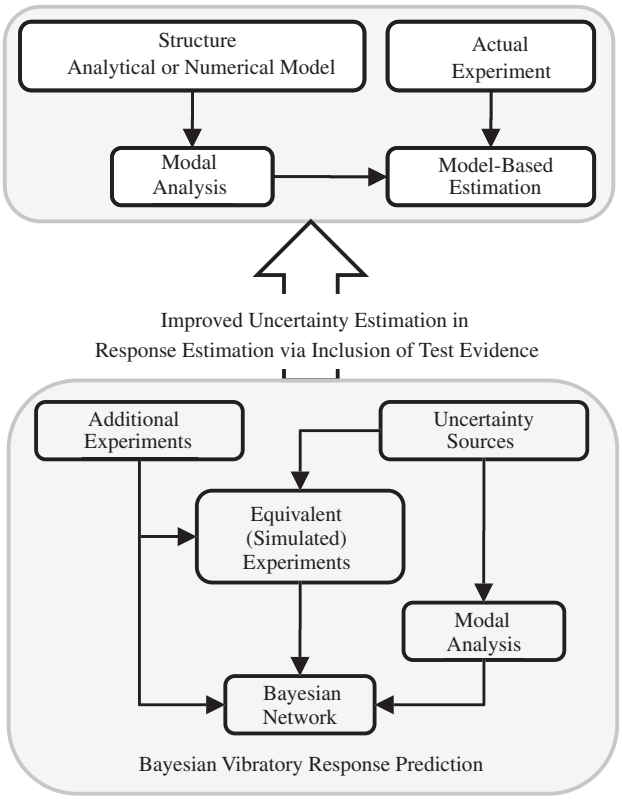

Fig. 1. Bayesian model-based vibratory response inference procedure.

This process has been investigated on the inference technique presented in [43], where a characterization of relevant types of uncertainties was also formulated. Pertinent information is also available in Refs. [42,44] which present feasibility studies on Bayesian networks and a quantitative assessment of experimental variability. In order to combine the information from forced-response experiments with the knowledge from modal analyses on the analytical model, and account for variability from both, a Bayesian representation of the given inference technique is herein constructed which permits the quantification and reduction of uncertainty as a function of the available experimental data. This process of integration is illustrated in Fig. 1 for which three fundamental steps can be identified:

- creation of an analytical/numerical experimentation model representing the given real/experimental conditions;
- establishment of a Bayesian network topology for response inference and population of its elements by means of the simulated experimental data;
- infusion of the real test data for the updating of the prior statistical information within the network.

Next, the simulation environment and the Bayesian network topology adopted for the assessment of a system's vibratory response are presented with the modal-based inference scheme applied separately to each resonance condition. As a result, the Bayesian network is also resonance-specific and computation of its prior information is needed at each of those conditions.

2.1. Equivalent numerical experimentation

The first step in the uncertainty-quantification process is the construction of a simulated-experiment environment (e.g., a finite-element forced-response analysis) equivalent to the actual test setup, where equivalency is defined in terms of comparable levels of uncertainty within the results generated via the numerical/analytical framework and the corresponding test data. In practical applications, not all the sources of uncertainty are detectable or observable, nor their impact can always be isolated in a comprehensive way. In this sense, simulated experimentation is not meant to duplicate reality, but rather to identify a set Θ^E of explanatory factors through which physical observations and corresponding uncertainties can be "equivalently" accounted for, even though such a set might not be at all exhaustive due

to analytical limitations as well as a lack of complete knowledge about the structure and its true state. In fact,

$$\Theta^E = \{\theta_i^E,\ i = 1,\ldots,N_E\} \subseteqq \Theta^{\mathrm{T}} = \{\theta_j^{\mathrm{T}},\ j = 1,\ldots,N_T\} \tag{2}$$

where Θ^{T} represents, instead, the set of quantities, often unknown, which fully describe the physical system and its inherent random nature. Given an analytical experiment environment, the method of direct propagation of input-parameter uncertainties can be used to identify suitable sets Θ^E for any specific structure and loading condition, as well as to establish the statistical cause–effect relationships necessary to construct a Bayesian network. Furthermore, this approach also serves the purpose of a screening test, as it pinpoints which parameters, among the ones being investigated, are mostly responsible for the variability in the system's response, and which ones could be neglected with minimal loss of information. Besides reducing the number of nodes to be modeled within a Bayesian network, a screening test also permits to exclude weak cause–effect arcs that are unresponsive to the propagation of evidence through them. This unresponsiveness leads to two main effects. On the one hand, a node whose connections to other nodes are weak can be updated effectively only through evidence infusion at that same node, as any information included at any other nodes will be damped out and will not propagate to it. For the same reason, evidence introduced at that node will also transfer weakly or not at all to its parent and child nodes and its effect will be therefore isolated. On the other hand, there is always the risk that the training procedure may establish a link between a pair of nodes which is stronger than that observed through the sensitivity analysis, thus explaining the variability in the data differently and leading to posterior probabilities for the network nodes that are unwarranted by the data.

According to the proposed response-estimation technique [43], in order to train a Bayesian network, data associated with both forced-response and modal analyses are to be generated. The commonly used approach of direct uncertainty propagation through Monte Carlo simulations may, however, incur a high computational cost, even for simple structures. Therefore, surrogate models based on standard polynomial interpolation [45] have been adopted to limit the number of finite-element analyses to be executed. In this context, spline interpolation was selected in the case of harmonic analyses also to alleviate the dependence upon the spectrum's frequency resolution $\delta\omega$. In fact, for a fixed value of $\delta\omega$, the accuracy with which the response at resonance is computed varies as a function of the values of the independent-parameter vector $\boldsymbol{\theta}^E = [\theta_1^E,\ldots,\theta_{N_E}^E]$. As a result, the peak response, computed at any given point on the structure, exhibits a non-continuous behavior with respect to $\boldsymbol{\theta}^E$ which hinders the use of a continuous analytical model to represent their relationship and smooth out the observed discontinuities. The use of spline interpolation proved to be more efficient than adjusting $\delta\omega$ for each separate finite-element analysis.

Once the surrogate models relating peak responses and modal quantities to the independent parameters are established, uncertainty can be propagated by assigning appropriate probability density functions to the elements of $\boldsymbol{\theta}^E$, and the corresponding Bayesian network can be populated and trained. More precisely, given a particular structure subject to an external harmonic load, let $\Delta\omega$ be the range of the excitation frequency ω, sampled at values $\overline{\omega}_s$ ($s = 1,\ldots,N_\omega$) and containing only one resonance condition at ω_p; also, let $(\boldsymbol{\theta}_1^E,\ldots,\boldsymbol{\theta}_{N_d}^E)$ be a N_d-case Design Of Experiments (DOE) on the N_E independent parameters comprising each $\boldsymbol{\theta}^E$ (e.g., material properties, geometric quantities and others). For the i-th ($i = 1,\ldots,N_d$) simulated experiment (i.e., a harmonic analysis), the computed sampled measurements $\varepsilon_g(\overline{\omega}_s,\boldsymbol{\theta}_i^E)$ at the sensor location $\mathbf{x}_g$ ($g = 1,\ldots,N_g$) are used as an input to a standard interpolating-spline scheme, herein indicated with the operator $\Upsilon_\omega[\cdot]$. As a result, the entire forced response can be constructed over the entire frequency domain $\Delta\omega$ and the p-th peak frequency $\omega_p(\boldsymbol{\theta}_i^E)$ for the i-th DOE run can be estimated together with its corresponding response peak amplitude $\varepsilon_g^p(\boldsymbol{\theta}_i^E)$:

$$\varepsilon_g^p(\boldsymbol{\theta}_i^E) = \max_{\omega\in\Delta\omega}\{\,\Upsilon_\omega[\varepsilon_g(\overline{\omega}_s,\boldsymbol{\theta}_i^E)]\} \tag{3}$$

Once the resonance conditions are computed for all the N_d cases, such information is utilized to construct other surrogate models, via the interpolation operator $\Upsilon_E[\cdot]$, whose validity is limited to the domain of $\boldsymbol{\theta}^E$ spanned by the design of experiments itself:

$$\varepsilon_g^p(\boldsymbol{\theta}^E) = \Upsilon_E[\varepsilon_g^p(\boldsymbol{\theta}_i^E)] \tag{4}$$

$$\omega_p(\boldsymbol{\theta}^E) = \Upsilon_E[\omega_p(\boldsymbol{\theta}_i^E)] \tag{5}$$

where $\omega_p(\boldsymbol{\theta}^E)$ and $\varepsilon_g^p(\boldsymbol{\theta}^E)$ represent, respectively, the functional dependences of the p-th resonance frequency, recorded at the g-th sensor location, and the corresponding peak amplitude of the response being considered (e.g., strain) upon the vector $\boldsymbol{\theta}^E$.

In the case of the natural frequencies and the modal quantities $e(\mathbf{x})$ (e.g., modal strains, modal displacements, etc.), surrogate models are established only in terms of $\boldsymbol{\theta}^E$ as those quantities are frequency independent. An example of the aforementioned process is illustrated in Figs. 2 and 3, for the cases of harmonic and modal strain amplitudes of a plate subject to a base excitation, respectively. The results were obtained via a grid-like 25-run design of experiments performed in a domain of $\boldsymbol{\theta}^E = [L, W]$, where L and W are the plate's length and width, respectively. Surrogate models based on polynomial interpolation have been observed to perform well for the various ranges of excitation frequency being considered, also in light of the linear-arc assumption embedded within linear Bayesian networks, according to which the

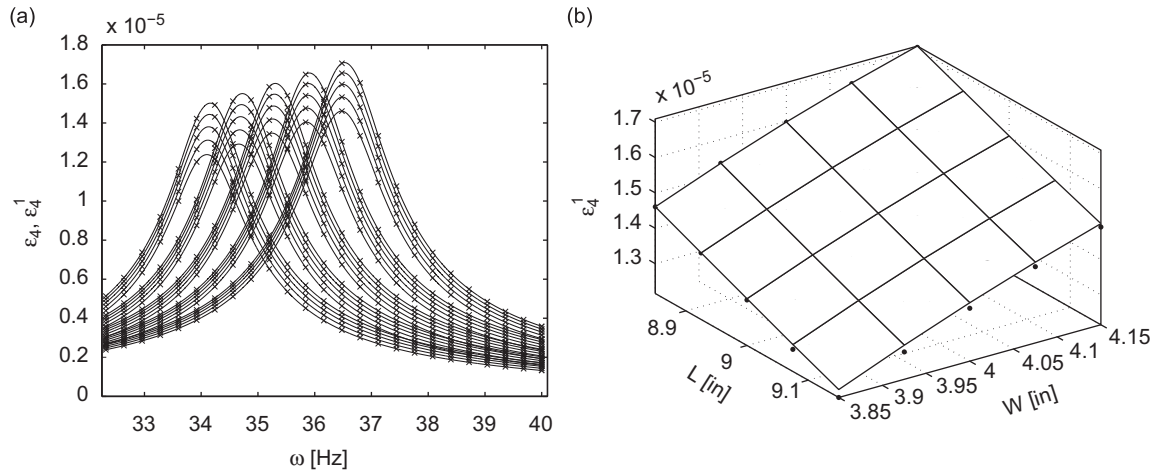

Fig. 2. Plate's strain amplitude ε_g at the g-th sensor location ($g=4$) and near the p-th resonance condition ($p=1$), computed for $N_d=25$: (a) 1D spline interpolation in the frequency domain and (b) 2D surrogate model in the domain $\Theta^E=\{L,W\}$. × Samples; • spline peaks of ε_4^1.

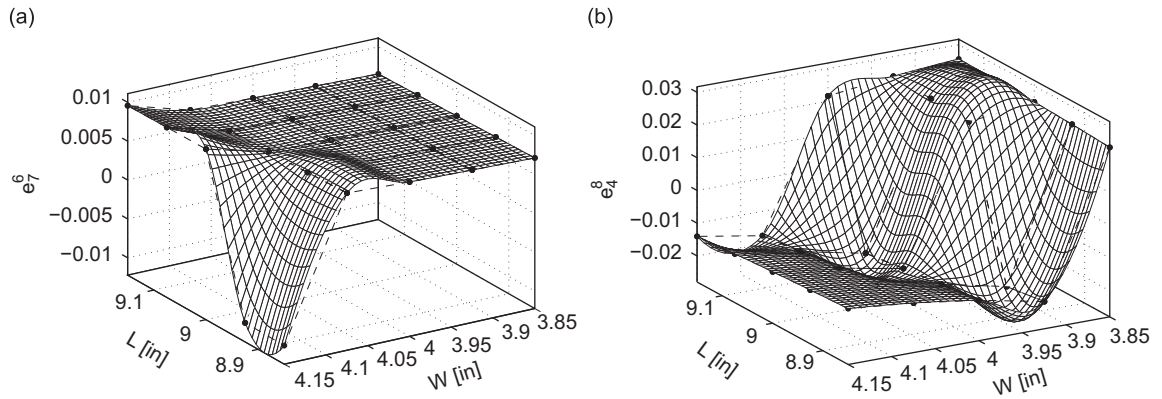

Fig. 3. Plate's modal strain amplitudes e_g^n, computed at the g-th sensor location for the n-th mode, computed for $N_d=25$: surrogate model in the domain $\Theta^E=\{L,W\}$ for (a) e_7^6 and (b) e_4^8.

statistical relationship between a node and its parent nodes is truncated to the first-order terms of its polynomial expansion. The size of the design of experiments needs to be adjusted depending on the excitation frequencies being considered and may need to be increased for higher frequency ranges to better capture stronger nonlinearities in the vibratory response and alleviate such issues like underfitting, even though the obtained accuracy may still not be good enough in the presence of strong gradients, as indicated by Fig. 3 in the case of the modal strain amplitudes for modes 6 and 8. Besides the issue of strong gradients, Fig. 3 also highlights the appearance of nodal regions within the domain of $\boldsymbol{\theta}^E$ for the given sensors. A sensor located in a nodal region usually yields both a low signal-to-noise ratio in the test measurements and numerical noise in the corresponding modal quantities. Therefore, such a sensor should not be modeled within the Bayesian network so as to avoid a loss in accuracy as well as singularities in the response prediction. Also to be excluded from the network are those sensors at whose locations the forced responses and/or the modal quantities of interest exhibit a very low sensitivity with respect to the independent variable $\boldsymbol{\theta}^E$. In fact, under these circumstances, the network training algorithm may not converge at all due to the presence of nodes with a very small variance behaving, in essence, as constant quantities rather than as random variables.

2.2. Bayesian network: topology selection and training

According to the inference scheme presented in [43], four groups of nodes can be herein identified for the n-th resonance and mode: the first group consists of independent quantities included in the set Θ^E and/or Θ^T, and describing the system's properties (e.g., material characteristics or geometric parameters) with respect to which the uncertainties under investigation are parameterized; the second set comprises the "modal nodes" (i.e., the modal ratios $e_{i\neq k}/e_k$ and e_M/e_k, and the natural frequency ω_n) identifying the modal quantities of interest, computed at the sensor locations ($1\leq i,k\leq N_g$) using gauge k as reference; the third group includes the "harmonic nodes" representing the computed and

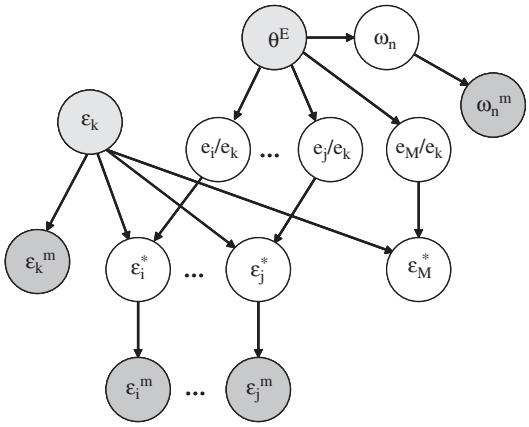

Fig. 4. Bayesian network topology.

estimated forced-response quantities (i.e., the true peak amplitude ε_k at the reference sensor k, the estimates $\varepsilon^*_{i\neq k}$ at the other locations, and the maximum-response estimate ε^*_M); and finally, the fourth set encompasses the "measurement nodes" (i.e., the sensor measurements ε^m_k, $\varepsilon^m_{i\neq k}$ at the recorded peak frequency ω^m_n), which consists of the actual outputs from the measuring devices.

Selection of the network's structure was driven by the impossibility of fully capturing Θ^{T}: all the factors responsible for the observed uncertainties may not be fully observable. The topology illustrated in Fig. 4 was adopted to model the response prediction scheme under uncertainty because of its ability to address the following issues:

- regardless of the parameters actually employed to generate the scatter in the simulated measurements, such variability can be ascribed to other factors as well, since none of the former ones is explicitly modeled in the network. This is in agreement with the idea of simulated experiments not being a duplicate of reality, but an equivalent representation of it;
- both measurement uncertainty and errors associated with the matching of the actual structure with a nominal model are consistently accounted for within the prediction scheme; and
- no hypothesis is necessary when constructing the network in terms of the completeness of the knowledge at hand (i.e., in practice $\Theta^E \subset \Theta^{\mathrm{T}}$ because of unobservable sources of uncertainties). Of course, the more information is available, the more educated the selection of the root nodes included in the set Θ^E can be, and the better the uncertainty can be quantified and reduced through evidence infusion.

Once the structure of the network is fixed, the next step is to populate its elements. Training data can be divided into two types: the first type includes the sample data obtained from the simulated modal and forced-response analyses, and used to establish the links among the root, the modal and the harmonic nodes; the second type contains the data that directly relates to the uncertainty embedded within the experimental measurements, which is responsible for how given computed nodes are connected to their measurement-node counterparts. The uncertainty propagated through the simulated experiments can be assigned based on the available expertise, or arbitrarily in the presence of limited knowledge (e.g., unknown tolerances associated with a particular manufacturing process), as long as the simulated response is comparable with the measured response in a statistical sense. The training data necessary to connect the measurement nodes to the rest of the network is a function of the error η associated with the particular instrumentation in use. In the case of Gaussian nodes, in agreement with the network's inherent nature, the measurement error η is also assumed to be normally distributed; hence, the following relationships are established for each physical quantity:

$$\varepsilon^m_k = \varepsilon_k + A_\varepsilon \eta_\varepsilon$$

$$\varepsilon^m_i = \varepsilon^*_i + A_\varepsilon \eta_\varepsilon \quad (i \neq k)$$

$$\omega^m_n = \omega_n + A_\omega \eta_\omega$$

$$\text{where} \quad \eta_\varepsilon \sim N(0, \sigma_\varepsilon)$$

$$\eta_\omega \sim N(0, \sigma_\omega) \tag{6}$$

The non-dimensional standard deviations σ_ε and σ_ω characterize, respectively, the variability in peak amplitude and peak frequency, while measurement accuracy is expressed in terms of the factors A_ε and A_ω whose values are chosen based on the scatter in the physical quantities due to uncertainty at the root-node level. In the ideal case of infinite

accuracy (zero σ's), the measurement nodes are a mere image of their counterparts and their links carry no additional statistical information; on the other hand, the higher the measurement errors embedded in the training data are (non-zero σ's), the more experimental uncertainty can be modeled in the network until a limit is reached at which the physical quantities and their measurements are no longer correlated, and their links actually destabilize the network.

In order to assess the network's ability to properly update itself upon evidence infusion, each node's assumed known true value is compared against the mean value of its posterior probability function. For a given true state [$\overline{\Theta}^E$, $\overline{e}_{i\neq k}/\overline{e}_k$, $\overline{e}_M/\overline{e}_k$, $\overline{\varepsilon}_k$, $\overline{\varepsilon}^*_{i\neq k}$, $\overline{\varepsilon}^*_M$, $\overline{\varepsilon}^m_k$, $\overline{\varepsilon}^m_{i\neq k}$, $\overline{\omega}_n$, $\overline{\omega}^m_n$] of the network and a specific evidence scenario (i.e., a subset of observed nodes), a metric δ has been adopted to evaluate how well the posterior mean μ of a queried node agrees with its assumed true state. For instance, for node ε_k and its true-state realization $\overline{\varepsilon}_k$, δ is defined as follows:

$$\delta = 100 \times \frac{\mu(\varepsilon_k) - \overline{\varepsilon}_k}{\Delta\varepsilon_k} \tag{7}$$

where $\Delta\varepsilon_k$ is the node's range of variability observed in the set of data used for validation. Similarly to ε_k, the percentage relative error δ can also be defined for all the other queried nodes in the network, defaulting to a value of zero for the observed nodes. Moreover, given a sample population of states, mean, standard deviation, and confidence intervals for each nodal δ can be obtained for any evidence scenario and can be used to assess the goodness of network updating in a statistical sense. Since only the measurement nodes are observable in an experiment, complete states for the network can only be computed by means of simulation, but their use in the computation of δ still provides valuable information in terms of the accuracy to be expected from the network when tracking the nodes' states associated with actual experimental observations.

In the following sections, the proposed methodology and its performance in quantifying uncertainty are investigated for a three-dimensional brass plate structure, where the system's vibratory performance was assessed in terms of maximum Von Mises strain.

3. Uncertainty quantification via continuous Gaussian nodes

Analyses on the response inference technique and its Bayesian-network implementation have been conducted on a one-dimensional beam as well as a three-dimensional structure. For the sake of clarity, results are presented only for the plate investigated in [42], instrumented with 11 strain gauges and subject to a base excitation. In this case, the system's response being tracked is in the form of surface strains, evaluated along the sensor measurement direction, while the Von Mises equivalent maximum strain represents the target quantity to be predicted. Errors associated with test measurements, uncertainty in model parameters, as well as the discrepancy in the correlation between the physical system and its model are all modeled within the network.

As a representative example, geometric uncertainty has been considered in the form of harmonic thickness variations along the plate's length L and width W. These particular parameters were utilized because they provide higher sensitivity for the vibratory response of the plate structure as compared to other sources of uncertainty. In a reference frame with z-axis perpendicular to the plate's main surfaces and origin coincident with one of its vertices, the following thickness tolerances, Δz_u and Δz_l, were assigned, respectively, on the upper and lower surfaces:

$$\Delta z_u(x,y) = +\frac{t_L}{2}\sin\left(2\pi\frac{y}{L}\right) + \frac{t_W}{2}\sin\left(2\pi\frac{x}{W}\right)$$

$$\Delta z_l(x,y) = -\frac{t_L}{2}\sin\left(2\pi\frac{y}{L}\right) - \frac{t_W}{2}\sin\left(2\pi\frac{x}{W}\right) \tag{8}$$

where t_L and t_W represent two Gaussian random variables with zero mean and standard deviations equal to 5 percent of the thickness nominal value 0.125 in.

In the first set of results, a four-gauge network was considered in which t_L was assumed to be the only source of uncertainty together with non-matching correlation between model and physical component. Hence, in the absence of measurement errors, the true-strain and predicted-strain nodes are connected to their corresponding measured-strain nodes by means of equality links. This setup allows to investigate the effect that the linear-link approximation has upon the network's ability to converge to the system's true state as a function of evidence. Despite the attempt at reducing nonlinearities by selecting, when possible, sensors at which the response exhibits shallow nonlinear trends, the major source of nonlinearity is embedded in the estimation process itself via the product of modal ratios and measurements.

The performance of the network with respect to evidence at the measurement nodes is illustrated in Fig. 5. In contrast with the desired behavior of the model, the error δ does not steadily decrease for all nodes with more evidence being infused into the network. Such a behavior is the result of fitting nonlinear data into a linearized model, basically an evidence-induced stiffening effect. As a consequence of this model underfitting, as more observations are added, the network loses some of its degrees of freedom, and it becomes incapable of explaining the new evidence, hence the rising of non-monotonic trends due to apparent conflicting information. Illustrated in Fig. 6 is the case in which evidence at the frequency node is included as the last observation. The frequency-measurement node influences primarily the modal nodes, while the forced-response ones are affected mostly by the amplitude-measurement nodes. No significant

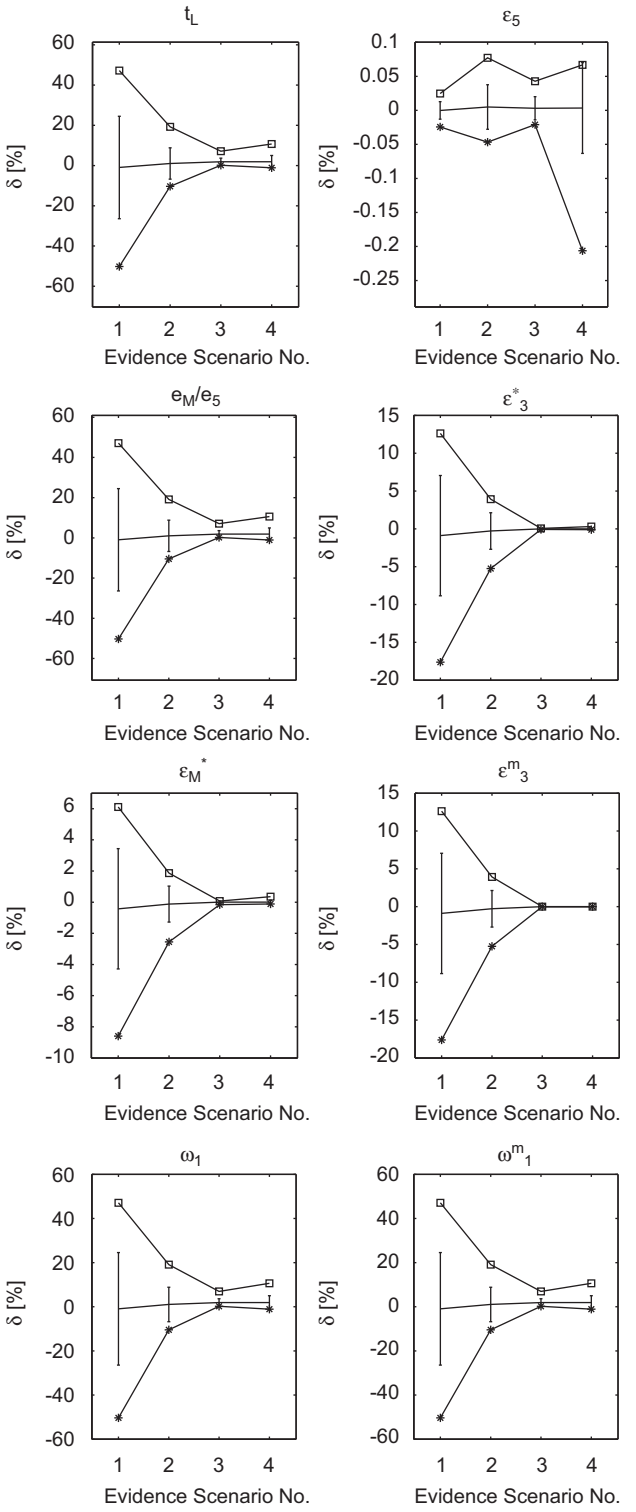

Fig. 5. Prediction error for the plate structure in the presence of uncertainty in t_L and no measurement errors, with evidence only at the amplitude measurement nodes of a four-gauge Bayesian network. — $\mu(\delta)\pm\sigma(\delta)$; $*$ min(δ); □ max(δ).

inconsistency arises from its addition, unless the $\pm 1\sigma$ interval for a specific node is already quite tight within a few percentage points. In the presence of measurement errors both in the training data and the observations, the network becomes more flexible with respect to evidence inclusion and an increasing number of sensors/observations becomes

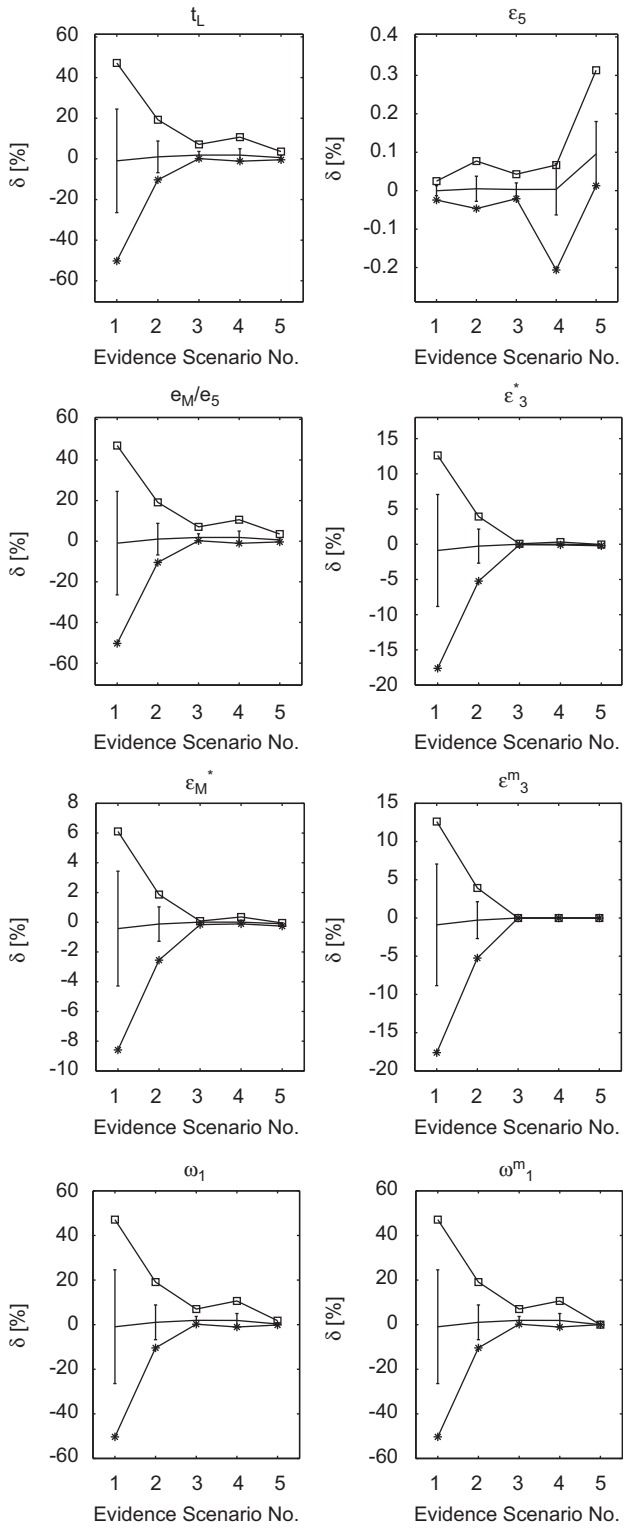

Fig. 6. Prediction error for the plate structure in the presence of uncertainty in t_L and no measurement errors, with evidence at the amplitude and frequency measurement nodes of a four-gauge Bayesian network. — $\mu(\delta)\pm\sigma(\delta)$; $*$ min(δ); □ max(δ).

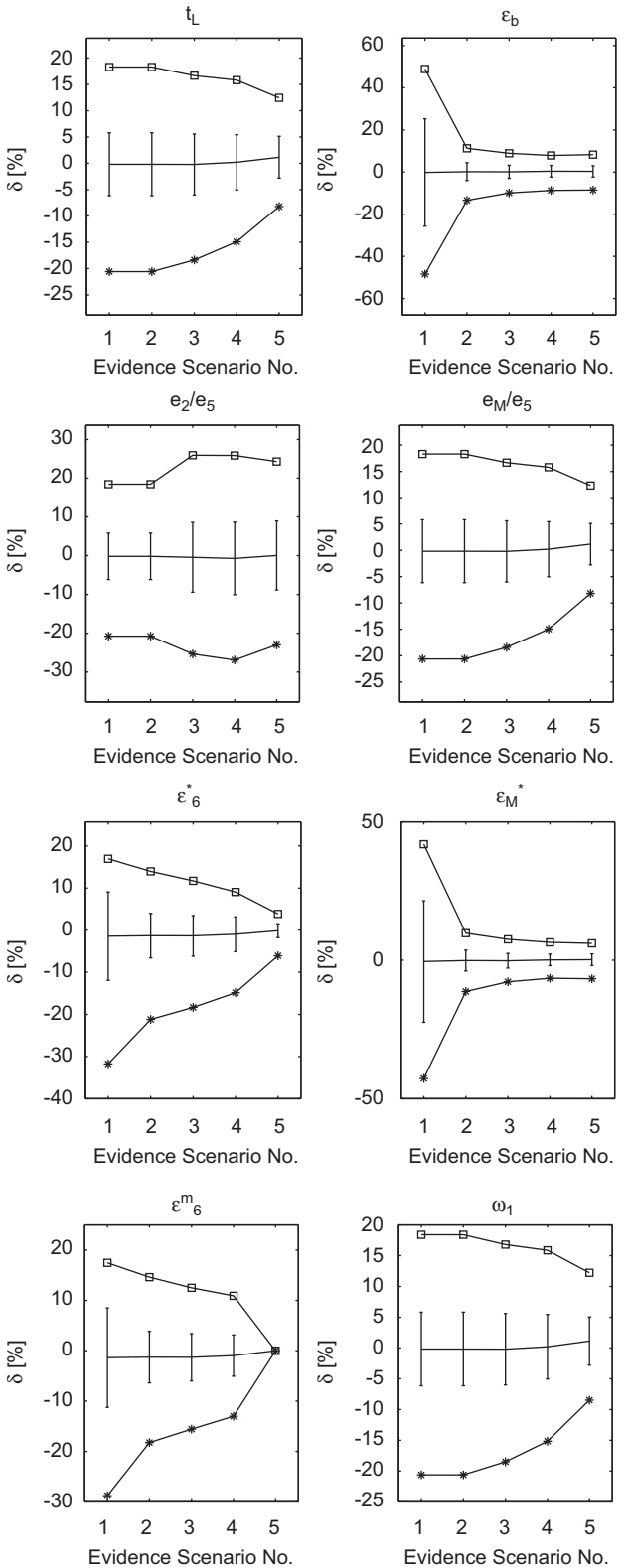

Fig. 7. Prediction error for the plate structure in the presence of uncertainty in t_L and measurement errors, with evidence at the amplitude and frequency measurement nodes of a four-gauge Bayesian network. — $\mu(\delta)\pm\sigma(\delta)$; $*$ min(δ); □ max(δ).

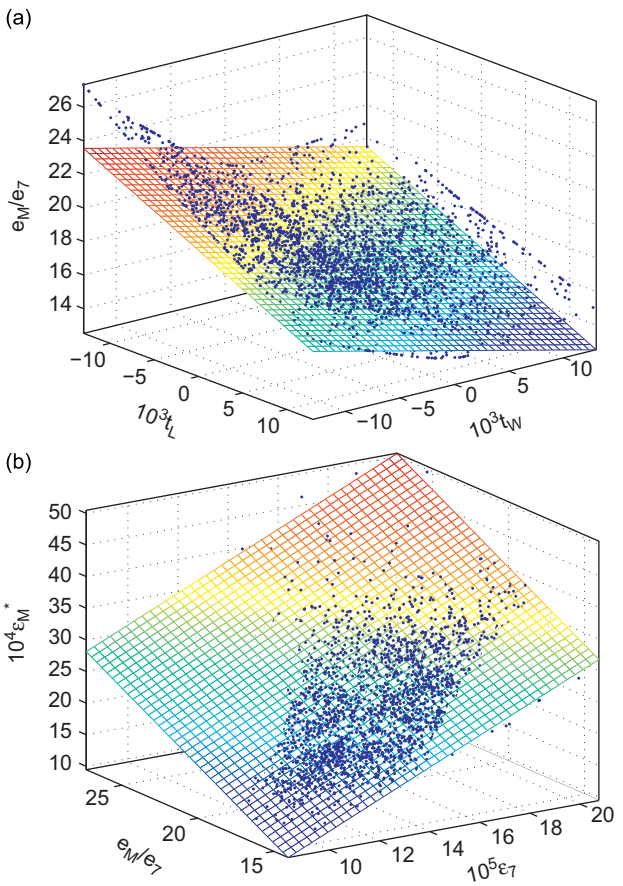

Fig. 8. Plate's data for network training and linear approximation for (a) e_M/e_7 and (b) ε_M^*. □ Linear Gaussian approximation; · data points.

beneficial in reducing the extra variability and consistently lowering the relative error δ, especially for the harmonic nodes (Fig. 7).

Another set of results is presented for the 20-node Bayesian network comprising t_L and t_W as root nodes together with five strain gauges. As indicated by Figs. 8 and 9, in spite of the nonlinearities affecting its links, the network performs satisfactorily as the discrepancy δ decreases with the infusion of more and more measurements. It is important to note that for the network to capture and properly quantify uncertainty, the error introduced by the linear approximation has to be lower than the one associated with other sources of variability. If a very low correlation between training data and linear models occurs, this results in meaningless cause–effect relationships being established among the nodes, and consequent poor performance of the network.

4. Discrete-node Bayesian networks

The results presented thus far were obtained using a Bayesian network comprised of continuous nodes and based upon the following assumptions:

- all the nodes are Gaussian variables;
- a node's Conditional Probability Distribution (CPD), describing the statistical dependency from its parent nodes, is a normal distribution whose mean is a linear function of the mean values of the parent nodes, and whose variance is fixed.

Gaussian nodes were chosen because their use leads to a closed-form solution of the marginal probability integrals and requires a lower computational cost as compared to utilizing other probability functions to describe the network nodes. Furthermore, other methods in the literature have also been successfully developed under the same assumption [25,26,46], motivated in part by the possibility of transforming, when desired, a set of non-normal random variables into an equivalent set of Gaussian ones via the Rosenblatt or the Nataf transformation [47].

Despite the fact that these assumptions are never met (e.g., for the prediction nodes alone, each $\varepsilon_{j\neq k}^*$ is not a linear combination of its parents and its distribution fails to be Gaussian even if its parents were normally distributed), the

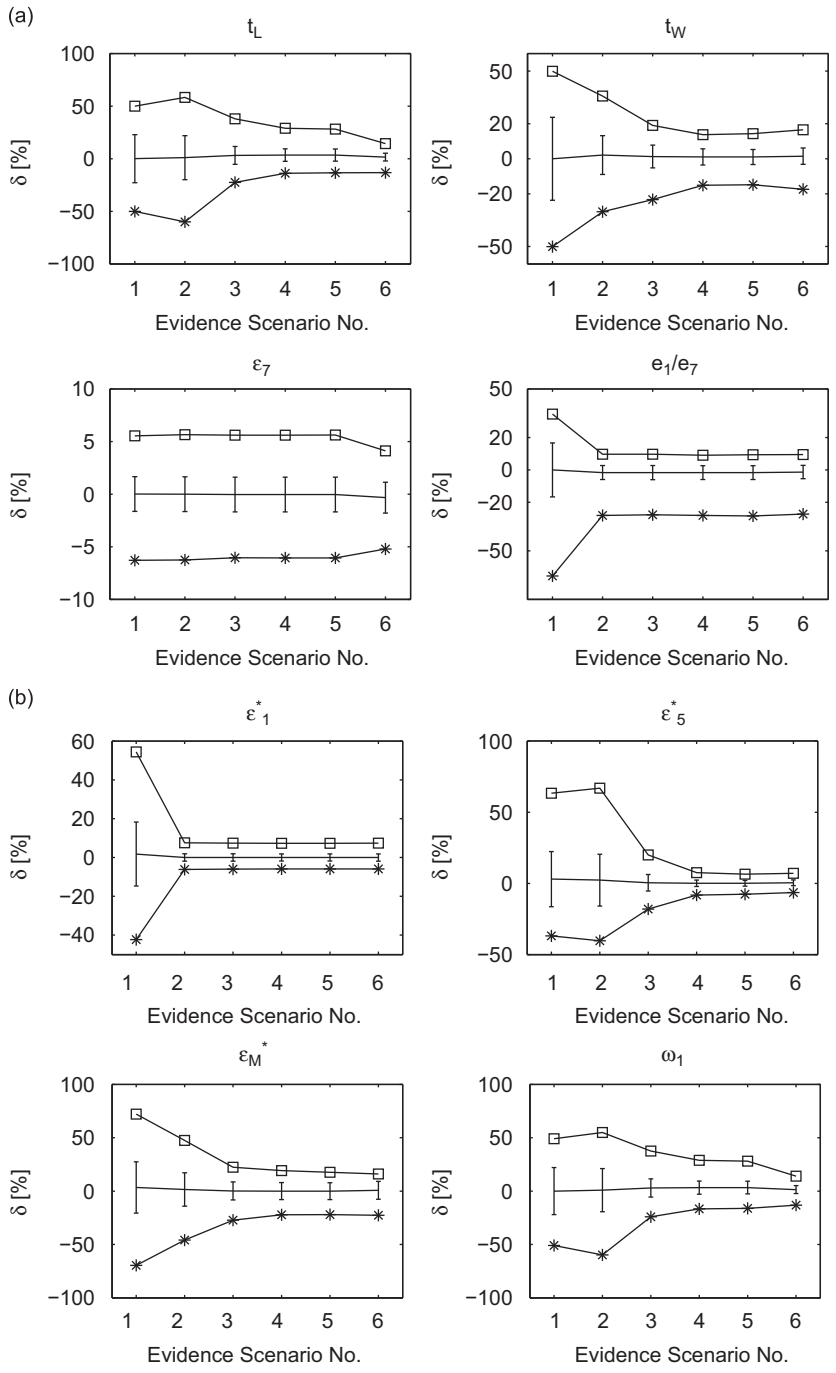

Fig. 9. Prediction error for the plate structure in the presence of uncertainty in t_L, t_W and the measurements, with evidence at the amplitude and frequency measurement nodes of a five-gauge Bayesian network. — $\mu(\delta)\pm\sigma(\delta)$; $*$ min(δ); □ max(δ).

previous results showed a satisfactory performance of the Bayesian inference scheme as long as the node-to-node links were not weakened by large approximation error due to excessive nonlinearities. Any significant non-Gaussian nature of the training data, instead, has not been taken into consideration in the previous analyses as it was neglected within the training procedure. In fact, the expectation-maximization learning algorithm in use within the BNT Gaussian toolbox trains the network by matching the first two moments (mean and standard deviation) of each node with the corresponding moments of the sample populations, regardless of their higher moments, which may still be statistically significant. Therefore, the use of a discrete-node Bayesian network was investigated to further assess the impact of the aforementioned assumptions upon the validity of the results.

Discrete-node Bayesian networks have both advantages and limitations. On the one hand, the discrete-node approach can be applied to any variable, independently of its underlying probability distribution, and the network's marginal probabilities can be inferred exactly (e.g., via the variable elimination algorithm, or by enumeration [48]) if the number of nodes is manageable. On the other hand, discretization of a continuous random variable inherently affects the level of detail in the results, which are now in the form of ranges of possible values and may lead to ambiguity if the true value of a continuous variable lies close to the border between two adjacent bins.

In the structural problems under investigation, the physical variables (e.g., geometric parameters, material properties, or stress field) are continuous in nature. In order to convert a continuous random variable X into a discrete node, a discretization into N_b states (also called bins) is performed. For each sampled node/variable X comprising the Bayesian network, the statistical results herein presented correspond to a six-bin discretization ($N_b = 6$), with the bins x_b ($b = 1,\ldots,N_b$) defined by the following intervals:

$$\begin{aligned} x_1 &= (-\infty, \mu(X) - 2\sigma(X)] \\ x_2 &= [\mu(X) - 2\sigma(X), \mu(X) - \sigma(X)] \\ x_3 &= [\mu(X) - \sigma(X), \mu(X)] \\ x_4 &= [\mu(X), \mu(X) + \sigma(X)] \\ x_5 &= [\mu(X) + \sigma(X), \mu(X) + 2\sigma(X)] \\ x_6 &= [\,\mu(X) + 2\sigma(X), \infty) \end{aligned} \tag{9}$$

where $\mu(\cdot)$ and $\sigma(\cdot)$ are, respectively, the mean and the standard-deviation operators applied to the sample population of X. The result of network training is independent of the nodes' level of discretization into bins, except for the size of the nodal Conditional Probability Tables (CPT's). In fact, the conditional probability $P(X = x|Y = y, Z = z)$ of a generic discrete node X and its discrete parents, Y and Z, is simply computed as follows:

$$\begin{aligned} P(X = x|Y = y, Z = z) &= \frac{P(X = x, Y = y, Z = z)}{P(Y = y, Z = z)} \\ &\approx \frac{\text{Number of times } X = x, Y = y \text{ and } Z = z \text{ in the sample population}}{\text{Number of times } Y = y \text{ and } Z = z \text{ in the sample population}} \end{aligned} \tag{10}$$

where x, y and z represent generic possible bins in which, X, Y and Z can be, respectively. Therefore, results for a coarser discretization could be obtained by proper combination of corresponding CPT entries and nodal marginal probabilities without having to resort again to network training.

An important issue to take into consideration in the discrete approach is the case in which certain combinations of states for the parents of a child node are never observed in the sample population. As a consequence of that, referring to Eq. (10), the joint probability of the parent nodes $P(Y = y, Z = z)$ cannot be defined using the information at hand. Such a scenario has a twofold explanation: on the one hand, the given combination of states has not been observed yet, but it could still be assumed as possible; on the other hand, such a combination cannot ever be observed because it represents an infeasible dynamic/vibratory state for the system. Possible solutions to such a situation could be the use of a coarser binning, specifying the conditional probability $P(X = x|Y = y, Z = z)$ according to some known probability function (e.g., the uniform distribution) for those CPT entries otherwise undefined, or introducing a fictitious state x^f for the given child X, whose conditional probability equals zero or one, respectively, for observed and unobserved/infeasible combinations of the parents' states:

$$P(X = x^f|Y = y, Z = z) = \begin{cases} 1 & \text{if } P(Y = y, Z = z) \text{ undefined} \\ 0 & \text{if } P(Y = y, Z = z) \text{ defined} \end{cases} \tag{11}$$

The above definition relies on the fact that the employed statistical algorithm assigns a default value of zero to any conditional probability which cannot be computed from the training data using Eq. (10). Therefore, Eq. (11) is intended as a possible alternative to resolve inconsistencies within a node's CPT. Since the number of fictitious states has no influence whatsoever on the nodes' marginal probabilities associated with the real states, but it only results in a larger-scale problem with no gain of information, only one fictitious state was added, per node, when needed.

Either approach could be adopted, each with some repercussions. On the one hand, the use of a different binning strategy causes a change in accuracy and might not necessarily resolve the underlying problem, especially when nodes at deeper network levels are involved, as more complex dynamic/structural interdependencies may be present. On the other hand, the usage of a known, yet arbitrary, probability function to handle undefined scenarios introduces an error in the marginal probabilities which spreads throughout all the states of the nodes, thus making it difficult to quantify its impact. Furthermore, the selection of another probability function will result in different amount and propagation of the error, thus calling for its selection in an appropriate fashion. The error associated with the introduction of a fictitious state, instead, can be quantified more easily because localized on that single state rather than distributed across all the bins, while its

marginal Probability Mass Function (PMF) value can be discarded because it contains no meaningful information. To this end, a normalized PMF $\tilde{P}$ for node X can be defined as follows:

$$\tilde{P}(X=x_i)=P(X=x_i)+\frac{P(X=x^f)\cdot P(X=x_i)}{\sum_{i=1}^{N_b}P(X=x_i)}$$

$$\text{where}\quad P(X=x^f)+\sum_{i=1}^{N_b}P(X=x_i)=1 \tag{12}$$

where x_i $(i=1,\ldots,N_b)$ and x^f are X's real and fictitious state, respectively. If, for a given evidence scenario, its marginal probability is not null, the presence of an artificial bin, *de facto*, induces a more conservative interpretation of the results, whereas the proportional normalization in Eq. (12) redistributes its probability, and allows for a more consistent comparison with other analyses (e.g., a continuous-node Bayesian network) in which no fictitious state may be present.

5. Uncertainty quantification via discrete nodes

When considering a network's response to evidence infusion, results showed that both the discrete-node network and the continuous-node one behave in a similar fashion, i.e., they exhibit the same qualitative sensitivity to the various evidence scenarios. The investigation also indicated that the network may not always be capable of pinpointing the true states, either because of the particular binning strategy or actual network limitations. On the one hand, the shifting of the bins be may be able to better clarify certain inconclusive probability distributions according to which no particular state may be identified as the most probable. On the other hand, the network may be incapable of matching the true states with the highest-probability bins, even though the introduction of evidence skews the probability mass functions towards the true states, thus permitting to exclude certain bins which are farther away.

In order to quantify the level of confidence to be associated with a given response estimate, a metric Π similar to δ was chosen for the discrete network as well. For each discrete node, Π_0 and Π_1 represent the rates of occurrence, respectively, that the bin with the highest posterior probability coincides with or is next to the true state. In other words, Π_0 and Π_1 are defined, respectively, in terms of zero-bin and one-bin distances between the highest-probability state and the true one. Illustrated in Fig. 10 are the results for the plate structure, where 3000 true network states were generated, and where observations were introduced, one at a time, first at the amplitude-measurement nodes and then at the frequency-measurement node. It can be observed that, if not coincident, the nodes' most probable bins are, at least, next to their true states in the largest majority of the cases. Therefore, in practical scenarios in which the true values of the structure's parameters and response are indeed unknown, a conservative prediction of the true states can be done by considering the highest-probability bin together with its immediate neighbors, where changes in the domain discretization can be carried out in an attempt to improve the confidence level associated with the estimated system's response. Finally, the trends shown for Π_0 in Fig. 10 for the root and modal nodes are in agreement with what observed for their continuous counterparts in Fig. 9. The observed similarity in behavior seems to indicate that the effect of evidence depends primarily on the structure of the training data and the topology of the network, regardless of how the random nodes are modeled. The quality of the prediction at those nodes, however, will depend on bin discretization and linear-approximation error for the discrete and the continuous network, respectively. Limitations in the identification of the correct true states, respectively as most probable bins or mean values, are also to be ascribed to the nonuniqueness of the solution at the root-node level.

6. Bayesian analysis of experimental data

Thus far, the performance of the network has been tested with respect to simulated data. The statistical metric δ has been used to quantify how well a randomly-generated assigned state of a structure agrees with its Bayesian expected state, as well as to assess whether or not convergence to that true state improves and uncertainty reduces as more sensor information is made available and infused into the network.

The next and final step consists of using real experimental data as observations for the measurement nodes. For this purpose, the same experimental data analyzed in [42] were utilized, where only 5 out of the 11 sensors (i.e., gauges 1, 3, 5, 7, and 9) were employed to construct the 20-node Bayesian network of Fig. 4. More specifically, gauges located near the plate's root and mid-length region were selected so as to include within the analysis different levels of signal-to-noise ratio, while also taking into consideration the nonlinear behavior of the strain field with respect to the uncertainties modeled at the root nodes. Furthermore, given the fact that variations in the plate's geometry (specifically, length, width and thickness), as well as in its modulus of elasticity, density and damping ratio were observed to generate little or no spread in the modal strain ratios and/or the forced strains, only t_L and t_W were adopted as independent parameters so that all the modal and harmonic nodes in the Bayesian network would be characterized by a meaningful level of variability.

For a specific experiment conducted on the brass plate, whose properties are listed in Table 1, results corresponding to the first resonance condition are presented in Table 2 and Figs. 11–13, where the Gaussian measurement errors η of Eq. (6) were considered with $\sigma_\varepsilon=0.01$ and $\sigma_\omega=\alpha$ $(\alpha=0,1,2$ percent); also, A_ε and A_ω were chosen to be equal to the maximum

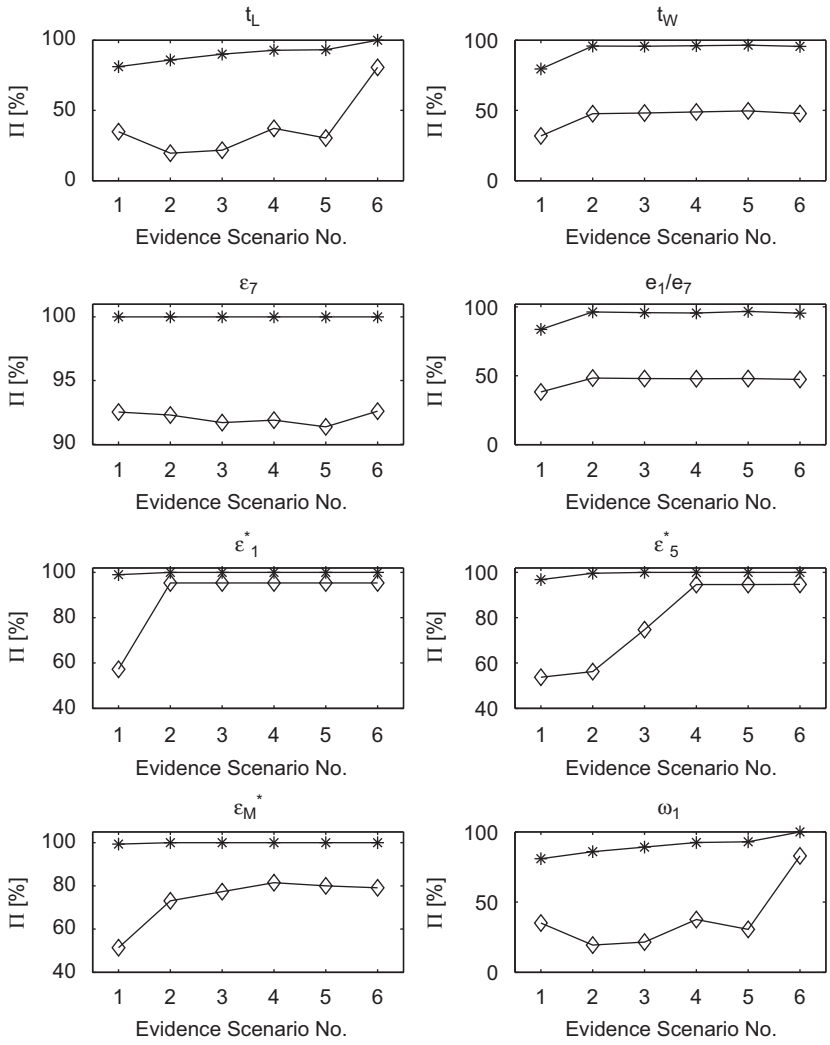

Fig. 10. Prediction rate of success Π for the plate structure in the presence of geometric uncertainty in t_L, t_W and measurement errors, with evidence at the amplitude and frequency measurement nodes of a five-gauge discrete Bayesian network. $\diamond$ Π_0; $*$ Π_1.

Table 1
Brass plate's material properties and geometry.

Quantity	Nominal value
Young's modulus E (psi)	15×10^6
Density ρ (lb/in^3)	0.3077
Poisson ratio v	0.34
Length L (in)	9
Width W (in)	4
Thickness T (in)	0.125

values observed in the training data for the strain peak amplitudes and frequency, respectively. Listed in the table are the results of the correlation analysis for the modeled sensors, where gauge 7 has been chosen as reference, and where a frequency-matching-based 20 percent reduction in the nominal value of Young's modulus has been included in an effort to improve the model/test correlation. In light of the large range of possible values in the material properties of brass [49], this correction appears to be reasonable and can prove to be beneficial when constructing equivalent numerical experiments, since the impact of evidence is inversely related to its distance from the prior information within the network. The definition of the correlation coefficient ξ_{ij} was given in [42] and relates the forced response at the i-th and j-th sensors

Table 2
Correlation Ξ for brass plate based on gauge 7.

Experiment vs. nominal system ξ_{17}	ξ_{37}		ξ_{57}		ξ_{97}
0.9111	0.7112		0.5180		0.5509
Evidence scenario no.	*Experiment vs. Bayesian network* Observed nodes	ξ^*_{17}	ξ^*_{37}	ξ^*_{57}	ξ^*_{97}
1	ε_7^m	0.9949	0.9964	0.9970	0.9970
2	ε_7^m, ε_1^m	1.0185	1.0105	1.0038	1.0025
3	ε_7^m, ε_1^m, ε_3^m	1.0693	1.0516	1.2017	1.1566
4	ε_7^m, ε_1^m, ε_3^m, ε_5^m	1.0393	1.1067	1.2899	1.2431
5	ε_7^m, ε_1^m, ε_3^m, ε_5^m, ε_9^m	1.0291	1.1169	1.3573	1.2244
6 ($\alpha = 0\%$)	ε_7^m, ε_1^m, ε_3^m, ε_5^m, ε_9^m,ω_1^m	0.7860	0.7088	0.5753	0.6041
6 ($\alpha = 1\%$)	ε_7^m, ε_1^m, ε_3^m, ε_5^m, ε_9^m, ω_1^m	0.8675	0.8285	0.7449	0.7556
6 ($\alpha = 2\%$)	ε_7^m, ε_1^m, ε_3^m, ε_5^m, ε_9^m, ω_1^m	0.9510	0.9683	0.9970	0.9617

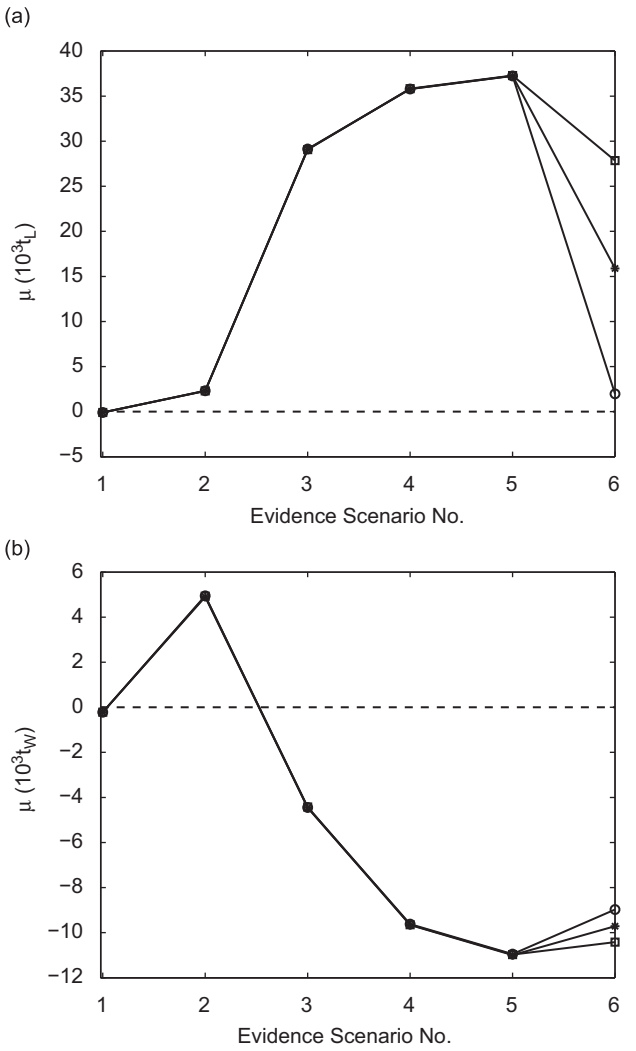

Fig. 11. Effect of evidence upon (a) t_L and (b) t_W of the brass plate in the presence of measurement errors, for a five-gauge Bayesian network. – – – – Nominal system; ○ $\alpha = 0\%$; ∗ $\alpha = 1\%$; □ $\alpha = 2\%$.

$(i=1,3,5,9;\ j=7)$ via their modal ratio corresponding to the nominal structure. A statistical correlation ξ^*_{ij} $(i=1,3,5,9;\ j=7)$ is, instead, defined as follows:

$$\xi^*_{ij}=\frac{\overline{\varepsilon}^m_j/\overline{\varepsilon}^m_i}{\mu\left(\dfrac{e_j}{e_i}\right)} \tag{13}$$

As discussed in [42], the non-unitary values of ξ_{ij} indicate that the measured response of the physical system is not always well correlated with the response computed analytically. Furthermore, correlation is not the same across the various gauge pairs, thus leading to different estimates of the system response, at other non-instrumented locations, depending on which sensors are used. As for ξ^*_{ij}, their values will depend on the amount of error present in the network, as indicated by the tabulated results obtained considering a constant error level in the amplitude measurements and varying error $N(0,\sigma_\omega)$ associated with the frequency measurement. For low error levels, the Bayesian network has less freedom to adjust itself and compensate for inconsistent evidence, whereas it is able to achieve better correlation between experimental data and analytical information as more uncertainty is present in the frequency measurement. This behavior is in agreement with what observed previously for the trend of the nodal δ's, with and without measurement errors which, *de facto*, provide the linear network with useful freedom to fit nonlinear information. Furthermore, in those cases in which the final correlation is deteriorated with respect to the nominal case, the network attempts to redistribute it across all sensors, thus reducing the response variability across the various pairs of gauges. For the same reasons, the correlation for certain sensors does not

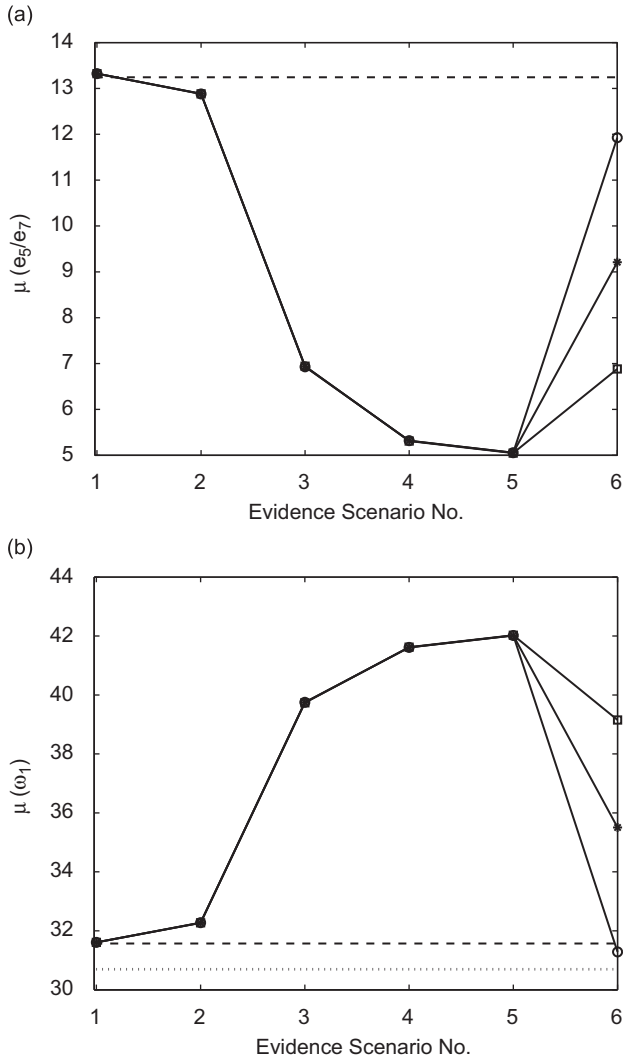

Fig. 12. Effect of evidence upon (a) e_5/e_7 and (b) ω_1 of the brass plate in the presence of measurement errors, for a five-gauge Bayesian network. – – – – Nominal system; ○ $\alpha=0\%$; ∗ $\alpha=1\%$; □ $\alpha=2\%$; ··· experiment.

vary monotonically as more observations are introduced because of the inconsistencies for which the network tries to compensate. The entire set of measurement evidence, therefore, is not only beneficial, but also necessary to guide the network towards a final expected state that agrees better with all the pieces of information.

The specific effect of observations upon the network's nodes is illustrated in Figs. 11–13, where the posterior expected values are also compared against the structure's nominal geometry and response obtained either analytically or estimated through a combination with the experimental data. As previously observed, for the independent geometric parameters and the modal nodes, evidence is not always capable of univocally matching the physical system's true state with their expected values. In the case of actual experimental evidence, this problem may be further exacerbated because of modeling limitations and more uncertainty being present in the physical system than the one actually captured by the equivalent numerical experimentation. On the one hand, in fact, the simple sinusoidal variations in thickness, introduced via Eq. (8), are only one possible way to account for the presence of manufacturing-induced geometric uncertainty, which may be distributed or concentrated in real components. On the other hand, the same geometric uncertainties become a surrogate for other non-modeled sources of uncertainty. In light of these issues, as shown in the figures, large deviations between the nominal model and the Bayesian expected model may appear, where the final expected states of all the nodes are, however, consistent with the experimental observations provided, and lead to a reduction in the variability of the maximum-response estimate, as indicated by the results of Table 3. The confidence level associated with those expected states is a function of the amount of error embedded in the experimental information itself, whose statistical significance and accuracy is weighed against the prior information in the network according to conditional probability theory. As a final

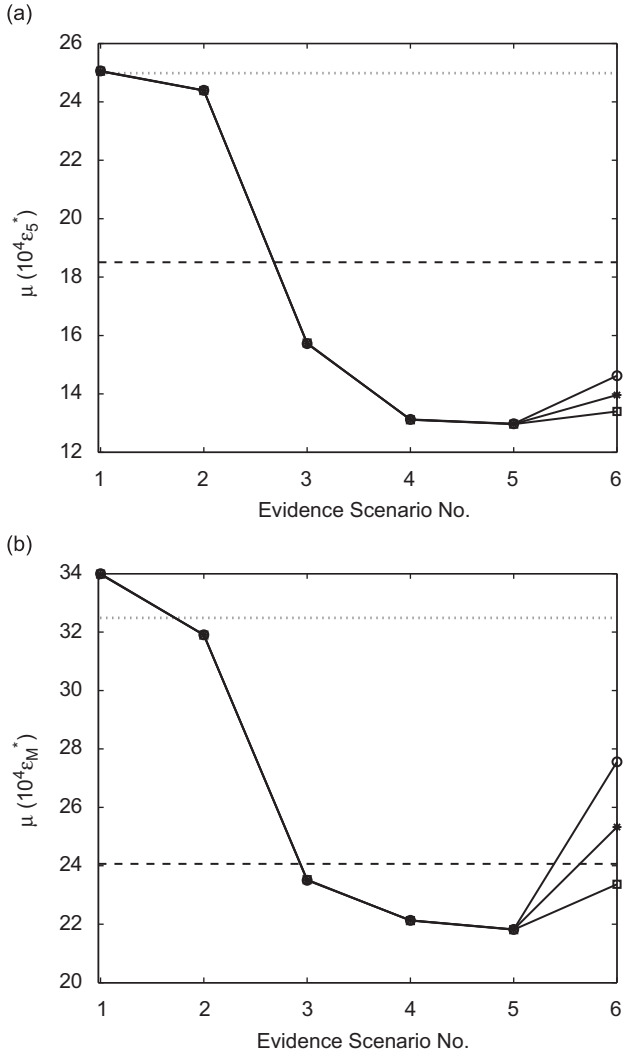

Fig. 13. Effect of evidence upon (a) $\varepsilon_5^*$and (b) ε_M^* of the brass plate in the presence of measurement errors, for a five-gauge Bayesian network. – – – – Nominal system; ○ $\alpha = 0\%$; ∗ $\alpha = 1\%$; □ $\alpha = 2\%$; · · · nominal system and experiment.

Table 3
Maximum-response estimation results.

Estimation via nominal model and experimental data					
	$i=1$	$i=3$	$i=5$	$i=7$	$i=9$
$\frac{e_{M_{\overline{\varepsilon}_i^m}}}{e_i}$	0.0030	0.0023	0.0017	0.0032	0.0018
Estimation via Bayesian expected states					
			$\alpha=0\%$	$\alpha=1\%$	$\alpha=2\%$
$\mu(\varepsilon_i^*)\mu\left(\frac{e_M}{e_7}\right)\mu\left(\frac{e_i}{e_7}\right)$	$i=1$		0.0028	0.0025	0.0022
	$i=3$		0.0026	0.0025	0.0023
	$i=5$		0.0023	0.0023	0.0024
	$i=9$		0.0024	0.0024	0.0023
$\mu(\varepsilon_M^*)$			0.0027	0.0025	0.0023

Results corresponding to the 6th evidence scenario.

note, the network infused with evidence successfully helps explain and filter out the variability in the maximum-response estimate which inevitably originates from a host of sources of uncertainty such as low signal-to-noise ratios, inaccurate solution averaging in high-gradient regions for the strain field, or interpolation errors introduced by spectrum analyses.

7. Conclusions

The use of a Bayesian network for the model-based inference of the vibratory response of a structure has been investigated as a possible means to evaluate the level of confidence that can be assigned to a given estimate in the presence of different sources of uncertainty. The approach has been demonstrated for a plate structure, for various sources of uncertainty, and for two different types of networks with discrete and Gaussian nodes. In terms of performance, both networks behaved similarly, as they both responded comparably to evidence infusion and pinpointed the same limitations in predicting certain nodes correctly. Overall, the use of linear Gaussian networks was found to be satisfactory for this particular type of inference in spite of the ''bending'' of its underlying hypotheses. In fact, the linearized modeling of the physical relationships retained the fundamental sensitivity to evidence by excluding non-contributing factors, as well as updating the maximum-response estimate regardless of inverse-problem issues at the root nodes. Discrete nodes were investigated in an effort to improve evidence efficacy and alleviate the impact of the training upon network's performance. Their use, however, resulted in no significant improvement that would outweigh their drawbacks.

The proposed methodology suggests the use of Gaussian Bayesian networks as a statistical surrogate model of the structural inference scheme since it permits to account for unobservable sources of uncertainty through the parameterization of alternative sources of error. Furthermore, the accuracy of prediction can be statistically assessed via numerical experimentation, and a confidence level can be assigned to each node's estimation for any set of available node observations. Evidence infusion has been proven to increase the quality of prediction in or without the presence of experiment-based errors, where the same errors were observed to become beneficial in helping estimate nonlinear quantities by means of a linear model. The importance of using additional test data has also been shown as well as the diverse impacts that amplitude and frequency measurements have on network updating. The former may be sufficient to predict successfully the maximum response, but the latter appears to be necessary to update the system's model parameters. This evidence-induced update at the root nodes did not always lead to an acceptable solution of the inverse problem, as intended in the context of model-updating. In fact, the methodology was aimed primarily at increasing the confidence level at the system's performance/output level, and the results showed that this objective can be achieved without precise inference of the root-node values. The generality of this conclusion, however, presents an interesting subject for future study.

To conclude, for the main purpose of statistically assessing the estimation of a system's vibratory response, experimental knowledge and model information have been integrated within a scheme which has demonstrated to work satisfactorily for the tested sources of uncertainty under the given set of network assumptions.

Acknowledgments

The research presented herein was supported by the Air Force Office of Scientific Research (AFOSR) Test & Evaluation Program (Grant # FA9550-05-1-0149). Special thanks go to Drs. Peter Cento and Charles Vining from the Arnold Engineering Development Center, Arnold Air Force Base, TN.

References

[1] O. Nelles, *Nonlinear System Identification: From Classical Approaches to Neural Networks and Fuzzy Models*, Springer, New York, NY, USA, 2001.
[2] K.J. Astrom, P. Eykhoff, System identification — a survey, *Automatica* 7 (2) (1971) 123–162.
[3] F. Kozin, H.G. Natke, System identification techniques, *Structural Safety* 3 (3–4) (1986) 269–316.
[4] N. Stander, K.J. Craig, H. Mullerschon, R. Reichert, Material identification in structural optimization using response surfaces, *Structural and Multidisciplinary Optimization* 29 (2) (2005) 93–102.
[5] C. Chang, T. Chang, Y. Xu, Adaptive neural networks for model updating of structures, *Smart Materials and Structures* 9 (1) (2000) 59–68.
[6] A.G. Chassiakos, S.F. Masri, Identification of structural systems by neural networks, *Mathematics and Computers in Simulation* 40 (5–6) (1996) 637–656.
[7] R. Haber, H. Unbehauen, Structure identification of nonlinear dynamic systems. A survey on input/output approaches, *Automatica* 26 (4) (1990) 651–677.
[8] G. Kerschen, K. Worden, A.F. Vakakis, J.C. Golinval, Past, present and future of nonlinear system identification in structural dynamics, *Mechanical Systems and Signal Processing* 20 (3) (2006) 505–592.
[9] H. Unbehauen, System identification methods using parameter estimation: a survey, *Annual Review in Automatic Programming*, Vol. 12, Berlin, East Germany, 1985, pp. 69–81.
[10] H. Unbehauen, G.P. Rao, Continuous-time approaches to system identification. A survey, *Automatica* 26 (1) (1990) 23–35.
[11] J.E. Mottershead, M.I. Friswell, Model updating in structural dynamics: a survey, *Journal of Sound and Vibration* 167 (2) (1993) 347–375.
[12] R.I. Levin, A.J. Lieven, Dynamic finite element model updating using simulated annealing and genetic algorithm, *Journal of Mechanical System and Signal Processing* 12 (1) (1998) 91–120.
[13] F. Qingguo, L. Aiqun, M. Changqing, Dynamic finite element model updating using meta-model and genetic algorithm, *Journal of Southeast University* 22 (2) (2006) 213–217.
[14] M. Link, C. Miodrag, Combining adaptive FE mesh refinement and model parameter updating, *Proceedings of the 18th International Modal Analysis Conference*, San Antonio, TX, USA, 2000, pp. 584–588.
[15] P. Eykhoff, *System Identification: Parameter and State Estimation*, Wiley, New York, NY, USA, 1974.
[16] J.L. Beck, L.S. Katafygiotis, Updating models and their uncertainties. I: Bayesian statistical framework, *Journal of Engineering Mechanics* 124 (4) (1998) 455–461.
[17] M.W. Vanik, J.L. Beck, S.K. Au, A Bayesian probabilistic approach to structural health monitoring, *Journal of Engineering Mechanics* 126 (2000) 738–745.
[18] L.S. Katafygiotis, J.L. Beck, Updating models and their uncertainties. II: Model identifiability, *Journal of Engineering Mechanics* 124 (4) (1998) 463–467.
[19] J. Ching, J.L. Beck, Bayesian analysis of the phase II IASC-ASCE structural health monitoring experimental benchmark data, *Journal of Engineering Mechanics* 130 (2004) 1233–1244.
[20] J. Ching, M. Muto, J.L. Beck, Structural model updating and health monitoring with incomplete modal data using Gibbs sampler, *Computer-Aided Civil Infrastructure Engineering* 21 (4) (2006) 242–257.
[21] H.F. Lam, L.S. Katafygiotis, N.C. Mickleborough, Application of a statistical model updating approach on phase I of the IASC-ASCE structural health monitoring benchmark study, *Journal of Engineering Mechanics* 130 (1) (2004) 34–48.
[22] K. Yuen, J.L. Beck, L.S. Katafygiotis, Unified probabilistic approach for model updating and damage detection, *Journal of Applied Mechanics* 73 (4) (2006) 555–564.
[23] K. Yuen, S.K. Au, J.L. Beck, Two-stage structural health monitoring approach for phase I benchmark studies, *Journal of Engineering Mechanics* 130 (2004) 16–33.
[24] K. Yuen, L.S. Katafygiotis, Model updating using noisy response measurements without knowledge of the input spectrum, *Earthquake Engineering and Structural Dynamics* 34 (2) (2005) 167–187.
[25] J.R. Fonseca, M.I. Friswell, J.E. Mottershead, A.W. Lees, Uncertainty identification by the maximum likelihood method, *Journal of Sound and Vibration* 288 (3) (2005) 587–599.
[26] M.I. Friswell, J.R. Fonseca, J.E. Mottershead, A.W. Lees, Quantification of uncertainty using inverse methods, *Proceedings of the 45th AIAA/ASME/ASCE/AHS/ASC Structures, Structural Dynamics and Materials Conference*, Vol. 3, Palm Springs, CA, USA, 2004, pp. 1756–1763.
[27] C. Mares, J.E. Mottershead, M.I. Friswell, Stochastic model updating: part 1 — theory and simulated example, *Mechanical Systems and Signal Processing* 20 (7) (2006) 1674–1695.
[28] J.E. Mottershead, C. Mares, S. James, M.I. Friswell, Stochastic model updating: part 2 — application to a set of physical structures, *Mechanical Systems and Signal Processing* 20 (8) (2006) 2171–2185.
[29] P. Geyskens, A. Der Kiureghian, P. Monteiro, Bayesian prediction of elastic modulus of concrete, *Journal of Structural Engineering* 124 (1) (1998) 89–95.
[30] T.K. Hasselman, Quantification of uncertainty in structural dynamic models, *Journal of Aerospace Engineering* 14 (4) (2001) 158–165.
[31] F. Hemez, S. Doebling, Model validation and uncertainty quantification, *Proceedings of the 19th International Modal Analysis Conference*, Kissimmee, FL, USA, 2001, pp. 1153–1158.
[32] S. Mahadevan, R. Rebba, Model predictive capability assessment under uncertainty, *Proceedings of the 46th AIAA/ASME/AHS/ASC Structures, Structural Dynamics and Materials Conference*, Austin, TX, USA, 2005, AIAA Paper No. 2005–2140, pp. 4196–4204.
[33] S. Mahadevan, R. Rebba, Validation of reliability computational models using Bayes networks, *Reliability Engineering and System Safety* 87 (2) (2005) 223–232.
[34] R. Rebba, S. Mahadevan, R. Zhang, Validation of uncertainty propagation models, *Proceedings of the 44th AIAA/ASME/ASCE/AHS Structures, Structural Dynamics and Materials Conference*, Vol. 6, Norfolk, VA, USA, 2003, pp. 4671–4678.
[35] R. Zhang, S. Mahadevan, Bayesian methodology for reliability model acceptance, *Reliability and System Safety* 80 (1) (2003) 95–103.
[36] M.I. Araujo, B. De Bragana Pereira, A comparison of Bayes factors for separated models: some simulation results, *Communications in Statistics — Simulation and Computation* 36 (2) (2007) 297–309.
[37] J.M. Van Noortwijk, H.J. Kalk, M.T. Duits, E.H. Chbab. The use of Bayes factors for model selection in structural reliability, *Proceedings of the 8th International Conference on Structural Safety and Reliability*, Newport Beach, CA, USA, 2001.
[38] J.L. Beck, K. Yuen, Model selection using response measurements: Bayesian probabilistic approach, *Journal of Engineering Mechanics* 130 (2) (2004) 192–2003.
[39] D.J.C. Mackay, Bayesian interpolation, *Neural Computation* 4 (3) (1992) 415–447.
[40] S.F. Gull, *Bayesian Inductive Inference and Maximum Entropy*, Kluwer, Boston, MA, USA, 1988, pp. 53–74.
[41] H. Jeffreys, *Theory of Probability*, Oxford University Press, Oxford, UK, 1939.
[42] G. Calanni Fraccone, M. Ruzzene, V. Volovoi, P. Cento, T. Tibbals, C. Vining, Investigation of sources of uncertainty for stress prediction in dynamic structures, *Proceedings of the 48th AIAA/ASME/ASCE/AHS/ASC Structures, Structural Dynamics, and Materials Conference*, Vol. 3, Honolulu, HI, USA, 2007, pp. 3181–3196.
[43] G. Calanni Fraccone, M. Ruzzene, V. Volovoi, P. Cento, C. Vining, Assessment of uncertainty in response estimation for turbine engine bladed disks, *Journal of Sound and Vibration* 317 (3-5) (2008) 625–645.
[44] G. Calanni Fraccone, V. Volovoi, M. Ruzzene, P. Cento, C. Vining, Quantification of uncertainty related to stress estimation in turbine engine blades, *Proceedings of the ASME Turbo Expo 2006 Conference*, Barcelona, Spain, 2006.
[45] The MathWorks™ Inc. © 1994–2008, Matlab, Software Package.

[46] K. Worden, T.M. Manson, T.M. Lord, M.I. Friswell, Some observations on uncertainty propagation through a simple nonlinear system, *Journal of Sound and Vibration* 288 (3) (2005) 601–621.
[47] R.E. Melchers, *Structural Reliability Analysis and Prediction*, second ed., Wiley, New York, NY, USA, 1999.
[48] P. Norvig, R. Stuart, *Artificial Intelligence: A Modern Approach, Prentice Hall Series in Artificial Intelligence*, second ed., Pearson Education, Upper Saddle River, NJ, USA, 2003.
[49] Matweb, Overview of materials for Brass, Automation Creations, Inc. © 1996–2008, Blacksburg, VA, USA.